

# Feasibility of first principles molecular dynamics in fault-tolerant quantum computer by quantum phase estimation

Ichio Kikuchi<sup>1</sup>, Akihito Kikuchi<sup>2\*</sup>

<sup>1</sup>Internationales Forschungszentrum für Quantentechnik

<sup>2</sup>International Research Center for Quantum Technology, Tokyo

May 16, 2024

## Abstract

This article shows a proof of concept regarding the feasibility of ab initio molecular simulation, wherein the wavefunctions and the positions of nuclei are simultaneously determined by the quantum algorithm, as is realized by the so-called Car-Parrinello method by classical computing. The approach used in this article is of a hybrid style, which shall be realized by future fault-tolerant quantum computer. First, the basic equations are approximated by polynomials. Second, those polynomials are transformed to a specific form, wherein all variables (representing the wavefunctions and the atomic coordinates) are given by the transformations acting on a linear space of monomials with finite dimension, and the unknown variables could be determined as the eigenvalues of those transformation matrices. Third, the eigenvalues are determined by quantum phase estimation. Following these three steps, namely, symbolic, numeric, and quantum steps, we can determine the optimized electronic and atomic structures of molecules.

## 1 Introduction

The authors of the present article have developed a method of quantum simulation of materials, wherein numeric, symbolic, and quantum algorithms are employed [1, 2, 3, 4]. This approach uses the following steps.

---

\*akihito.kikuchi@gakushikai.jp (The corresponding author; a visiting researcher in IFQT)

- The molecular integrals are given by analytic functions generated from analytic atomic bases, such as GTO or STO, through the standard method of computational chemistry [5, 6].
- The energy is given by an analytic function. It is a multivariate polynomial, where the variables represent the coefficients of LCAO. In the same way, the ortho-normalization condition for the wavefunctions is prepared with Lagrange multipliers that represent orbital energies. If necessary, through the series expansion for other variables in the function, extra unknowns are included in the polynomial objective function for the total energy.
- A system of polynomial equations is derived according to the minimum condition of the energy functional.

$$f_1 = f_2 = \dots = f_t = 0 \quad (1)$$

Those polynomials are represented by the coefficients of LCAO, the orbital energies, and other variables, say, the atomic coordinates. Henceforward, assume that those variables are represented by  $x_1, x_2, \dots$ , and  $x_n$ .

- The polynomials in the system of equations compose an ideal  $I$  in a suitable commutative ring  $R = C[x_1, x_2, \dots, x_n]$ , where  $C$  is the number field. Then the Gröbner basis  $G$  for  $I$  can be computed [7, 8, 9, 10, 11].  $G$  and  $I$  are equivalent in such a way that the zeros of these two systems depict the same geometric object in the Cartesian coordinate space.
- An ideal  $I$  in the commutative algebra could be decomposed as the intersection of primary ideals [7]:

$$I = \bigcap_i p_i$$

Each primary ideal in the decomposition stands for a smaller subset of the original system of polynomial equations. By finding out the common zero set of the polynomials in each subset, we get a part of the roots of the originally given problem. Note that the decomposition of the ideal is a counterpart of the prime factorization of an integer:  $n = p_1^{a_1} p_2^{a_2} \dots p_n^{a_n}$ .

- The quotient ring  $R/I(= R/G)$  should be zero-dimensional. Namely, the system of polynomial equations, represented by the corresponding Gröbner basis, has discrete roots.
- We use the following algorithm [12].

- Let  $\bar{x}_1, \bar{x}_2, \dots, \bar{x}_2$  be the representatives of  $x_1, x_2, \dots, x_n$  in  $R[x_1, x_2, \dots, x_n]/G$ . Additionally, let  $b$  be a vector that is composed of the representatives of the monomial basis of the quotient ring.
- For any  $i$ , the multiplication  $\bar{x}_i \cdot b$  is represented by

$$\bar{x}_i \cdot b = b \cdot M_{x_i} \quad (2)$$

with a transformation matrix  $M_{x_i}$ . The entries of the matrix are numbers, but not symbols.

- As  $M_{x_i} \cdot M_{x_j} = M_{x_j} \cdot M_{x_i}$ , those transformation matrices share common eigenvectors  $\{v_j | j = 1, \dots, N_M\}$ , where  $N_m$  is size of the monomial basis  $b$ .
- Let us consider the eigenvalue problems, defined as follows,

$$\bar{\xi}_i^{(j)} v_j = v_j \cdot M_{x_i} \quad (3)$$

for  $i = 1, \dots, m$  and  $j = 1, \dots, N_M$ . Those equations are solved numerically, and the eigenvalues give the common zero set of the polynomials included in the ideal  $I$ . Namely, the eigenvalues give the roots of the set of polynomial equations in such a way that

$$f_1(\bar{\xi}_1^{(j)}, \bar{\xi}_2^{(j)}, \dots, \bar{\xi}_n^{(j)}) = f_2(\bar{\xi}_1^{(j)}, \bar{\xi}_2^{(j)}, \dots, \bar{\xi}_n^{(j)}) = \dots = f_i(\bar{\xi}_1^{(j)}, \bar{\xi}_2^{(j)}, \dots, \bar{\xi}_n^{(j)}) = 0 \quad (4)$$

for  $j = 1, \dots, N_M$ . Note that if eigenvectors  $\{v_j\}_j$  for one of the  $\{M_i\}_i$  is obtained, the other components of the roots are computed by

$$\bar{\xi}_i^{(j)} = \frac{(v_j \cdot M_{x_i}, v_j)}{(v_j, v_j)}. \quad (5)$$

Each solution  $(\bar{\xi}_1^{(j)}, \bar{\xi}_2^{(j)}, \dots, \bar{\xi}_n^{(j)})$  corresponds to a primary ideal  $p_i$  in the primary ideal decomposition of the ideal  $I = (f_1, \dots, f_i) = \bigcap_i p_i$ .

- The quantum phase estimation (QPE) computes the eigenvalues of those transformation matrices. The common eigenvector  $|v_j\rangle$  of those matrices is encoded in the quantum states and the eigenvalues of the matrices  $\{\bar{\xi}_i^{(j)}\}_i$  are successively recorded in the ancillary component. Namely, the result of the computation shall be encoded in a quantum state as follows:

$$|v_j\rangle |0\rangle |0\rangle \dots |0\rangle \xrightarrow{QPE} |v_j\rangle \left| \bar{\xi}_1^{(j)} \right\rangle \left| \bar{\xi}_2^{(j)} \right\rangle \dots \left| \bar{\xi}_n^{(j)} \right\rangle \quad (6)$$

As the transformation matrices are not Hermitian, their time evolution should be executed by special quantum circuits, wherein a matrix  $A$  is embedded in the leading principal block of a larger unitary matrix  $U$  acting on the full Hilbert space:

$$U = \begin{pmatrix} A & * \\ * & * \end{pmatrix} \quad (7)$$

This sort of unitary operation is realized in a quantum circuit by the trick of block encoding [13], as is illustrated in Figure 1. The block-encoding of  $A$  in  $U$  enables us to put an arbitrary state vector in the input and execute the matrix-vector multiplication:  $A|v\rangle$ . Consequently, the time-evolution  $\exp(-\sqrt{-1}A)$  for the non-Hermitian matrix  $A$ , which is required in the QPE, is implemented in a quantum circuit.

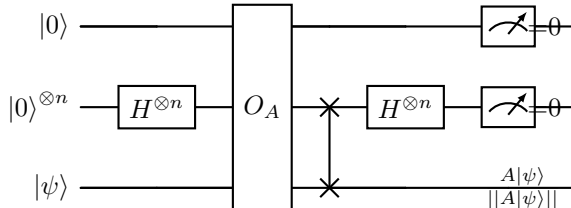


Figure 1: An illustration of the quantum circuit that executes block-encoding. The circuit is composed of Hadamard gates, the oracle  $O_A$ , and a swap gate. The query operation  $O_A$  for a  $2^n \times 2^n$  matrix  $A = \{a_{ij}\}$  is given by  $O_A|0\rangle|i\rangle|j\rangle = \left( a_{ij} |0\rangle + \sqrt{1 - |a_{ij}|^2} |1\rangle \right) |i\rangle|j\rangle$ . After the measurement, the quantum circuit generates  $\frac{A|\psi\rangle}{\|A|\psi\rangle\|}$ . Note that the block-encoding is applied only for the matrix that satisfies  $|a_{ij}| \leq 1$  for all entries. If the matrix  $A$  does not satisfy this condition, it should be multiplied by a suitable factor beforehand.

In the next section, we show how to apply this computational scheme in the determination of any degrees of freedom involved in the problem, since the potential ability of this approach is not limited to the computation of wavefunction.

## 2 The numerical experiment

### 2.1 The model description

We study a simple molecule  $\text{H}_3^+$ , as is shown in Figure 2. The shape of the molecule is an equilateral triangle with edge length  $R$ . Note that this molecule has attracted the interests of researchers in various fields since this molecule is the simplest triatomic molecule and abundant in the universe; this molecule is regarded as a benchmark problem of quantum chemistry [14, 15, 16, 17, 18, 19, 20, 21, 22, 23, 24]. The electronic structure of this molecule as an algebraic variety is analyzed by the authors of the present works [3].

As a test problem, we pick up the simultaneous determination of the optimum electronic and atomic structures of this molecule. As the symbolic computation consumes computational resources, we simplify the problem by using the symmetric character of the molecule. Then the problem is reduced to the question of solving the model with three variables,

which represent the essential elements in the molecular simulation, namely, a wavefunction, an orbital energy, and a bond length.

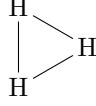


Figure 2: The molecular structure of  $H_3^+$

We adopt the following model.

- To study the electronic structure of the molecule using molecular orbital theory, we use the STO-3G basis as the atomic orbital bases, from which we construct the energy function of the restricted Hartree-Fock model. In the present case, we have only to consider only one molecular orbital. Namely, the degrees of the freedom of the system are given by the LCAO coefficients of three  $1s$  orbitals  $(x, y, z)$  the orbital energy  $e$ , and the bond length  $R$ . The necessary analytic formulas are given in the supplementary part of the present article. The symbolic computations to make up molecular integrals were carried out by a Python library *SymPy* [25].
- As we try to optimize the wave function and the atomic positions, the total energy is approximated by a truncated series representation (the Taylor expansion) for  $R$ . We choose the center of the expansion at  $R_c = 1.8 a_0$  and take the terms up to the third order of  $R$ .
- The coefficients in the total energy (with the constraint)  $\{C_i\}_i$  are replaced by fractional numbers  $\{D_i/10^n\}_i$  with a common denominator  $10^n$ . In this approximation, we set  $n = 8$ . Then we multiply the total energy (with the constraint) by  $10^n$  so that we use the objective function with integer coefficients.
- We simulate the ground state of the molecule, by setting  $x = y = z$ . In other words, the atomic orbitals in the three atomic sites have equal LCAO coefficients.

With these conditions, the multivariate polynomial approximation of the objective function is given by:

$$\begin{aligned}
 \text{OBJ} = & -25940329R^3e^x - 61451313R^3x^4 + 65640150R^3x^2 - \\
 \leftrightarrow & 28577961R^3 + 81961639R^2e^x + 1099859207R^2x^4 - \\
 \leftrightarrow & 811868595R^2x^2 + 205761316R^2 + 342231572Re^x - \\
 \leftrightarrow & 5233649558Rx^4 + 3595948148Rx^2 - 55555556R - 1960143305e^x - \\
 \leftrightarrow & + 200000000e + 8467967598x^4 - 6382868964x^2 + 666666666
 \end{aligned}$$

## 2.2 The validity of the approximation

First, we check the validity of the polynomial approximation for the objective function. Figure 3 shows the dependence of total energy on  $R$  for three cases: (1) the exact energy function, (2) the polynomial approximation made by the series expansion for  $R$ , and (3) the polynomial approximation with the coefficients with fractional numbers, which is given in the present section. Those three results coincide well at the neighborhood of  $R_c = 1.8$ , around which the minimum of the energy functional is located.

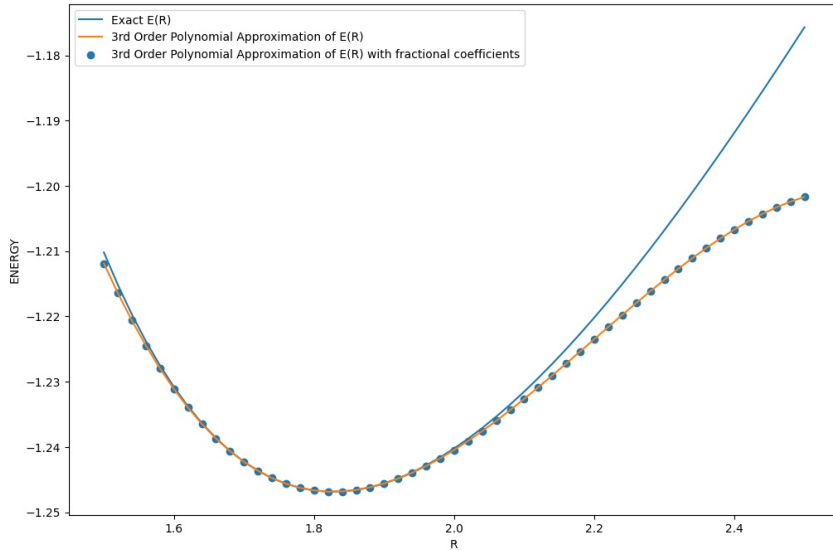


Figure 3: The total energy  $E(R)$  and the bond length  $R$  of  $\text{H}_3^+$ , computed by different levels of approximations: (1) the exact function (2) the polynomial approximation made by the series expansion for  $R$  (3) the polynomial approximation with approximated coefficients given by fractional numbers.

## 2.3 Symbolic and numeric computation

Second, we seek the optimum using numeric and symbolic algorithms. The optimum is given by the partial derivatives of the total energy with respect to  $x$ ,  $e$ , and  $R$ . In this step, we work in the ring  $\mathbf{Q}[x, e, R]$ , where the coefficient field is the rational number field. The monomial ordering is first given by the degree reverse lexicographic type, and then it is switched to the lexicographic type. (In the last monomial ordering, the Gröbner basis could be decomposed into a set of triangular systems, and the roots of the given equations could be evaluated in each of those triangular systems. This type of numerical algorithm yields the same results as the eigenvalue approach that is demonstrated later.) The authors of the present article used the GAP system [26] for symbolic computations related to Gröbner

basis.

The entries of the polynomial ideal  $I$  and the Gröbner basis  $G$  are not given here, since they are lengthy and complicated. The raw data are available via the internet. See the link given in Section 4.

The monomial basis  $bs$  of the quotient field  $\mathbf{Q}[x, e, R]/I$  is composed of the following elements.

```
bs={ xe4, ye4, x3eR, x2yeR, xy2eR, y3eR, xye2R, y2e2R, xe3R, ye3R, e4R,
↪ x3R2, x2yR2, xy2R2, y3R2, x2eR2, xyeR2, y2eR2, xe2R2, ye2R2, e3R2,
↪ xyR3, y2R3, xeR3, yeR3, e2R3, xR4, yR4, eR4, R5, x4, x3y, x2y2, xy3,
↪ y4, x3e, x2ye, xy2e, y3e, x2e2, xye2, y2e2, xe3, ye3, e4, x3R, x2yR,
↪ xy2R, y3R, x2eR, xyeR, y2eR, xe2R, ye2R, e3R, x2R2, xyR2, y2R2, xeR2,
↪ yeR2, e2R2, xR3, yR3, eR3, R4, x3, x2y, xy2, y3, x2e, xye, y2e, xe2,
↪ ye2, e3, x2R, xyR, y2R, xeR, yeR, e2R, xR2, yR2, eR2, R3, x2, xy, y2,
↪ xe, ye, e2, xR, yR, eR, R2, x, y, e, R, 1 }
```

The basis  $bs$  generates a vector space of 22 dimensions. The transformation matrices, which represent the multiplication of  $x$ ,  $y$ , and  $e$  over the monomial basis, are shown in the appendix. They are sparse, but not Hermitian.

$ i\rangle$	$x$	$e$	$R$	$E_{TOTAL}$	Type
0	-0.0000+0.2451j	25.1507+0.0000j	-4.4726-0.0000j	170.3683+0.0000j	complex
1	-0.0000-0.2451j	25.1507-0.0000j	-4.4726+0.0000j	170.3683-0.0000j	complex
2	0.6014+0.0000j	-1.8051+0.0000j	-3.8703+0.0000j	8.1743+0.0000j	real
3	-0.6014+0.0000j	-1.8051+0.0000j	-3.8703+0.0000j	8.1743+0.0000j	real
4	0.3703+0.0000j	-11.7442+0.0000j	-3.1022+0.0000j	21.7662+0.0000j	real
5	-0.3703+0.0000j	-11.7442+0.0000j	-3.1022+0.0000j	21.7662+0.0000j	real
6	0.1137+0.1795j	-0.6013-1.1800j	0.1264-1.6890j	0.9417+3.7454j	complex
7	0.1137-0.1795j	-0.6013+1.1800j	0.1264+1.6890j	0.9417-3.7454j	complex
8	-0.1137-0.1795j	-0.6013-1.1800j	0.1264-1.6890j	0.9417+3.7454j	complex
9	-0.1137+0.1795j	-0.6013+1.1800j	0.1264+1.6890j	0.9417-3.7454j	complex
10	0.4050+0.0000j	-1.1482+0.0000j	1.8272+0.0000j	-1.2469+0.0000j	real
11	-0.4050+0.0000j	-1.1482+0.0000j	1.8272+0.0000j	-1.2469+0.0000j	real
12	-0.4580+0.0000j	-0.8673+0.0000j	2.6811+0.0000j	-1.1895+0.0000j	real
13	0.4580+0.0000j	-0.8673+0.0000j	2.6811+0.0000j	-1.1895+0.0000j	real
14	-0.4790-0.0187j	-0.9176-0.5313j	2.8486-0.6587j	-1.2421+0.0174j	complex
15	-0.4790+0.0187j	-0.9176+0.5313j	2.8486+0.6587j	-1.2421-0.0174j	complex
16	0.4790+0.0187j	-0.9176-0.5313j	2.8486-0.6587j	-1.2421+0.0174j	complex
17	0.4790-0.0187j	-0.9176+0.5313j	2.8486+0.6587j	-1.2421-0.0174j	complex
18	-0.1775-0.3575j	-0.5221+0.8834j	2.9857-0.4501j	1.6144+2.1018j	complex
19	-0.1775+0.3575j	-0.5221-0.8834j	2.9857+0.4501j	1.6144-2.1018j	complex
20	0.1775+0.3575j	-0.5221+0.8834j	2.9857-0.4501j	1.6144+2.1018j	complex
21	0.1775-0.3575j	-0.5221-0.8834j	2.9857+0.4501j	1.6144-2.1018j	complex

Table 1: The list of the solutions. Each row, indexed by  $i = 0, \dots, 21$ , shows the computed value of  $x$ ,  $e$ ,  $R$ , the total energy, and the type of the solutions (real or complex). We use the symbol  $j$  to denote the imaginary unit.

In Table 1, the result of the computation is shown. The rows in the table show the sequential numbers of the normalized eigenvectors  $|i\rangle$  of the transformation matrix  $m_x$  (for  $i=0, \dots, 21$ ), the expectation values  $x = \langle i|m_x|i\rangle$ ,  $e = \langle i|m_e|i\rangle$ ,  $r = \langle i|m_r|i\rangle$ , the corresponding total energy, and the type of the solutions (real or complex).

We should discard the solutions of complex values and adopt only the real solutions. Moreover, we should assess the real solutions. As the most hazardous approximation in the computation is the series expansion with respect to  $R$ , we should seek the solutions that fall in the proper range of this approximation. We could guess that  $|10\rangle$  and  $|11\rangle$  would be appropriate solutions because  $\langle 10|m_r|10\rangle$  and  $\langle 11|m_r|11\rangle$  are located at the values closest to the center of the series expansion (given by  $R_c = 1.8$ ). Indeed they are the points where

the energy functional takes the minimum value.

In this way, the atomic coordinates and the wavefunctions could simultaneously be determined in a run. The potential supremacy of the algorithm described here is that the present scheme does not require any iterative numerical computations to achieve the self-consistency and the optimum of the energy.

As for the position of the center of the polynomial expansion, we can choose it in the range from 1.6 to 2.0 and we can reproduce the optimum almost equal to the one obtained in the above computation.

## 2.4 Quantum computation

In this section, we discuss how to compute the roots of the given equation using quantum phase estimation. We do not design the full circuit of the QPE, for the design of the QPE circuit is mere routine work. We focus on the construction of the quantum gate that carries out the time evolution since it is the key component of the algorithm.

As the matrices obtained in the present study are not Hermitian, we should use modified versions of QPE which could treat complex eigenvalues, as have been proposed by several authors [27, 28, 29]. These algorithms commonly use the trick of block-encoding, by which an arbitrary matrix  $A$  is embedded in a larger unitary matrix  $U$ . In this section, we use the FABLE method [13] to implement the block-encoding of the transformation matrices  $m_x$ ,  $m_y$ , and  $m_z$  in quantum circuits.

Let us investigate the reliability of the block encoding in the present study.

Table 2 shows the accuracy of the block encoding. It is evaluated by the square norms of the difference between the transformation matrix  $A$  and the top-left diagonal part  $A_{BL}$  in the Hermitian matrix  $U$  generated by the block-encoding:  $\|A - A_{BL}\|^2$ . The computed residues are almost zero.

	$M$	$\ M - M_{BL}\ $
0	$m_x$	1.938105e-24
1	$m_e$	7.236860e-22
2	$m_r$	2.597125e-22
3	$\exp(-i m_x)$	1.800854e-24
4	$\exp(-i m_y)$	3.391753e-21
5	$\exp(-i m_r)$	3.794574e-21

Table 2: The accuracy of block-encoding for the transformation matrices  $m_x$ ,  $m_y$ , and  $m_z$ . The difference between the matrix and the upper-left block of the unitary matrix of the corresponding block encoding are computed as the measures of the accuracy.

Table 3 shows the solutions of the optimization of the molecule  $\text{H}_3^+$ . In this case, instead of the transformation matrices used in the previous section, we used the emulation of the quantum circuit that conducts the block encoding. The result in this table agrees well with the result by the classical algorithm given in Table 3)

$ i\rangle$	x	e	R	ETOTAL	Type
0	-0.0000-0.2451j	25.1507-0.0000j	-4.4726-0.0000j	170.3683-0.0000j	complex
1	-0.0000+0.2451j	25.1507+0.0000j	-4.4726+0.0000j	170.3683+0.0000j	complex
2	0.6014-0.0000j	-1.8051-0.0000j	-3.8703-0.0000j	8.1743-0.0000j	real
3	-0.6014+0.0000j	-1.8051-0.0000j	-3.8703-0.0000j	8.1743-0.0000j	real
4	-0.3703+0.0000j	-11.7442-0.0000j	-3.1022-0.0000j	21.7662+0.0000j	real
5	0.3703-0.0000j	-11.7442-0.0000j	-3.1022-0.0000j	21.7662+0.0000j	real
6	-0.1137-0.1795j	-0.6013-1.1800j	0.1264-1.6890j	0.9417+3.7454j	complex
7	-0.1137+0.1795j	-0.6013+1.1800j	0.1264+1.6890j	0.9417-3.7454j	complex
8	0.1137+0.1795j	-0.6013-1.1800j	0.1264-1.6890j	0.9417+3.7454j	complex
9	0.1137-0.1795j	-0.6013+1.1800j	0.1264+1.6890j	0.9417-3.7454j	complex
10	-0.4050+0.0000j	-1.1482-0.0000j	1.8272-0.0000j	-1.2469-0.0000j	real
11	0.4050-0.0000j	-1.1482-0.0000j	1.8272-0.0000j	-1.2469+0.0000j	real
12	-0.4580+0.0000j	-0.8673-0.0000j	2.6811-0.0000j	-1.1895+0.0000j	real
13	0.4580-0.0000j	-0.8673-0.0000j	2.6811-0.0000j	-1.1895+0.0000j	real
14	-0.4790+0.0187j	-0.9176+0.5313j	2.8486+0.6587j	-1.2421-0.0174j	complex
15	-0.4790-0.0187j	-0.9176-0.5313j	2.8486-0.6587j	-1.2421+0.0174j	complex
16	0.4790-0.0187j	-0.9176+0.5313j	2.8486+0.6587j	-1.2421-0.0174j	complex
17	0.4790+0.0187j	-0.9176-0.5313j	2.8486-0.6587j	-1.2421+0.0174j	complex
18	-0.1775-0.3575j	-0.5221+0.8834j	2.9857-0.4501j	1.6144+2.1018j	complex
19	-0.1775+0.3575j	-0.5221-0.8834j	2.9857+0.4501j	1.6144-2.1018j	complex
20	0.1775+0.3575j	-0.5221+0.8834j	2.9857-0.4501j	1.6144+2.1018j	complex
21	0.1775-0.3575j	-0.5221-0.8834j	2.9857+0.4501j	1.6144-2.1018j	complex

Table 3: The list of the solutions computed from the block-encoded matrices. The solutions are presented in the same way as in Table 1.

Table 4 shows the check of the accuracy of the block encoding of the time-evolution operators ( $\exp(-1jA)$ ) for matrices  $A$ , by computing the expectation values of  $\exp(-1jA)$ . The block encoding yields quantitatively accurate results.

Operator	$ 10\rangle$	$ 11\rangle$
$m_x$ (Block Encoding)	0.4050-0.0000j	-0.4050+0.0000j
$m_e$ (Block Encoding)	-1.1482-0.0000j	-1.1482-0.0000j
$m_r$ (Block Encoding)	1.8272-0.0000j	1.8272-0.0000j
$\exp(-i m_x)$ (Block Encoding)	0.9191-0.3940j	0.9191+0.3940j
$\exp(-i m_e)$ (Block Encoding)	0.4102+0.9120j	0.4102+0.9120j
$\exp(-i m_r)$ (Block Encoding)	-0.2536-0.9673j	-0.2536-0.9673j
$\exp(-i x)$ (Direct)	0.9191-0.3940j	0.9191+0.3940j
$\exp(-i e)$ (Direct)	0.4102+0.9120j	0.4102+0.9120j
$\exp(-i R)$ (Direct)	-0.2536-0.9673j	-0.2536-0.9673j

Table 4: The accuracy of the block encoding for time evolution operators. The columns in this table show the expectation values of the operators  $m_x$ ,  $m_e$ ,  $m_r$ ,  $\exp(-i m_x)$ ,  $\exp(-i m_e)$ , and  $\exp(-i m_r)$  by the eigenvectors  $|10\rangle$  and  $|11\rangle$  in Table 1. The results are computed by two modes: (A) the block encoding and (B) the direct substitution of actual values of  $x$ ,  $e$ , and  $R$  to  $\exp(\cdot)$ . The results by block-encoding and the direct substitution are distinguished by the signs (Block Encoding) and (Direct). The results of these two modes of the computations agree well.

The numerical experiments given in Table 2, Table 3, and Table 4 affirm the accuracy of the block-encoding. We could determine the wavefunction and the atomic coordinates simultaneously by the quantum algorithm, provided that the given problem is transformed into a suitable form for quantum computations. To detect the optimum solution, we could use the same check for the computed value of  $R$ , as was used in the computation by the classical algorithm in the previous section.

To conclude this section, let us briefly review how the algorithm to evaluate complex eigenvalues works, using the method proposed in [28]. It is an extension to the standard QPE [30]. We assume the following conditions: the eigenvector  $|\psi_j\rangle$  for the operator  $U = \exp(2i\pi A)$  has the eigenvalue  $\lambda_j = |\lambda_j|e^{i2\pi\phi}$ , such that  $|\lambda_j| \leq 1$ ; the binary representation of  $\phi$  is given by  $(0.x_1x_2 \cdots x_m)$ . We could fulfill the first requirement  $|\lambda_j| \leq 1$  by multiplying a scale factor with the matrix  $A$  under investigation.

- We give the initial input of the iterative QPE as

$$|\Psi\rangle_i = |0\rangle_p |0 \cdots 0\rangle_a |\psi_j\rangle \quad (8)$$

- To determine a digit of  $\phi(x_k)$ , after several gate operations, we get the following state:

$$|\Psi\rangle_f \sim \left( (1 + e^{i2\pi(0.x_k)}|\lambda|^{2^k})|0\rangle_p + (1 - e^{i2\pi(0.x_k)}|\lambda|^{2^k})|1\rangle_p \right) |0 \cdots 0\rangle_a |\psi_j\rangle \quad (9)$$

- The measurement of the amplitudes on  $|0\rangle_p$  and  $|1\rangle_p$  enables us to determine  $x_k$  and  $|\lambda|$ , thanks to the following facts.

If  $x_k = 1$ , then

$$|\Psi\rangle_f \sim \left( (1 - |\bar{\lambda}|^{2k}) |0\rangle_p + (1 + |\bar{\lambda}|^{2k}) |1\rangle_p \right) |0 \cdots 0\rangle_a |\psi_j\rangle \quad (10)$$

In this case, since  $|1 - |\lambda|^{2k}| < |1 + |\lambda|^{2k}|$ , the probability to observe the state  $|1\rangle$  is larger.

If  $x_k = 0$ , then

$$|\Psi\rangle_f \sim \left( (1 + |\bar{\lambda}|^{2k}) |0\rangle + (1 - |\bar{\lambda}|^{2k}) |1\rangle \right) |0 \cdots 0\rangle_a |\psi_j\rangle \quad (11)$$

In this case, the probability of observing the state  $|0\rangle$  is larger.

In both cases, we can evaluate  $|\lambda|^{2k}$  from the measured amplitudes of  $|0\rangle_p$  and  $|1\rangle_p$ . As is pointed out in [28], when  $k$  grows larger, the difference between the amplitudes of  $|0\rangle_p$  and  $|1\rangle_p$  becomes smaller. This circumstance increases the difficulty of judging the correct  $x_k$ . However, in the problem discussed in the present article, it would not matter much: what we have to compute with precision are the real eigenvalues; regarding the complex ones, we have only to detect and discard them by rough estimation.

### 3 Summary and discussion

In this article, we have investigated the feasibility of first-principles molecular dynamics using quantum phase estimation. The algorithm used in this study is composed of the symbolic part and the quantum algorithmic part. In the symbolic part, we construct the set of matrices whose eigenvalues give the root of the governing equation in the given problem. In the quantum algorithmic part, we use the quantum phase estimation to compute the eigenvalues. We have verified that this scheme works well at least in the Hartree-Fock case for simple molecules, wherein we can determine the optimal configuration of the nuclei and the wavefunction simultaneously.

To conduct more quantitative calculations, the correction to electronic correlation, such as configuration interaction (CI), would be necessary. This sort of advanced theory is equally represented by polynomials, and our algorithm has the potential to treat it. In [3], we discussed the computation of virtual states that would be located above the ground state molecular orbitals. Those virtual orbitals could be encoded in quantum states lying on the qubits. Following a similar way, we could compute the virtual states, and compose the CI eigenvalue problem, which would be represented by polynomials. Moreover, for the effective computation of eigenvalues by QPE, we should use recent refined methods of time-evolution [31, 32, 33] and we should improve the techniques to prepare adequate eigenstates for QPE, such as proposed in [34, 35, 36, 37, 38, 32, 39, 40].

To improve the reliability of the algorithm explained in the present article, we should exploit related techniques, such as fault-tolerant quantum computation (FTQC) [41, 42], error correction and quantum code [43, 44, 45, 46, 47, 48]. In the studies of algebraic quantum codes, the ideas from number theory, algebraic topology, and discrete mathematics are commonly used [49, 50, 51, 52, 53]. The connection between quantum mechanics, number theory, discrete mathematics, and algebraic geometry, would be an important theme in the future. Such research shall pave the way for a full-fledged FTQC and also provide us with various topics that should be studied by trustworthy FTQC.

We make a short comment on the extension of the algorithm, by which the quantum dynamics of the nuclei could be simulated. In the present article, we have expressed the total energy of the molecule as a multivariate function composed of the atomic coordinate, the wave function, and the orbital energy. We treated the atomic positions as coordinate points in the context of classical dynamics. However, the algorithm presented in this article could get over this restriction. The wavefunction of the molecule could be given by the direct product of the nuclear and electronic parts

$$|\Psi\rangle = |\phi_{nuc}\rangle |\psi_{el}\rangle \quad (12)$$

The total energy in the model treated in this article shall be given by

$$\begin{aligned} E_{tot} &= \langle \Psi | \left( -\frac{1}{2\mu} \frac{\partial^2}{\partial^2 R} + H_{el}(R) \right) | \Psi \rangle \\ &= \langle \phi_{nuc} | \left( -\frac{1}{2\mu} \frac{\partial^2}{\partial^2 R} \right) | \phi_{nuc} \rangle + \langle \phi_{nuc} | (E_{el}(\psi, R)) | \phi_{nuc} \rangle \end{aligned} \quad (13)$$

In the above,  $H_{el}(R)$  is the electronic Hamiltonian and  $E_{el}(\psi, R)$  is the polynomial representation of the electronic energy. The dynamics related to the atomic coordinate are expressed by an additional kinetic term with a fictitious mass parameter  $\mu$ . As  $E_{el}(\psi, R)$  is the polynomial of  $R$ , the expectation value  $\langle \phi_{nuc} | (E_{el}(\psi, R)) | \phi_{nuc} \rangle$  is analytically computed when  $\phi_{nuc}$  is represented by the Gaussian-type basis set. Then  $E_{tot}$  is also the polynomial given by the LCAO coefficients of the nuclei and electron wavefunctions, and one can study it in a similar way that we have demonstrated. We could determine the energetic minimum, or we could draw the *orbit* of  $R$  when we set  $E_{tot} = E_r$  with an arbitrary value of the energy.

Note that the present article proposes another way of data preparation before the quantum computation. In chemical problems, one usually adopts the Wigner transformation, or other methods akin to it, to transform the Hamiltonian into a suitable form for the quantum algorithm. In other words, it is always necessary to rewrite the fundamental equations for the sake of the quantum algorithm, and this task requires a symbolic computation. In the case of the Wigner transformation, the cost for the symbolic computation is small. On the other hand, the method used in the present article requires the symbolic processing of polynomials. Therein the computational costs for generating Gröbner basis, in the worst cases,

would scale exponentially with the number of variables [54]. However, we could anticipate that the problem related to the algorithmic complexity of Gröbner basis computation might be mitigated by the parallel character of the quantum computations that could be conducted in the vast expansion of data space held on qubits. The authors of the present article hope that the seminal ideas used in our study will flourish in the coming era of fault-tolerant quantum computer.

## 4 Data availability

The programs used in this study and the result of the computation are available on the authors' GitHub:

<https://github.com/kikuchiichio/20240314>

## References

- [1] Akihito Kikuchi. An approach to first principles electronic structure computation by symbolic-numeric computation. *QScience Connect*, 2013:14, 2013. <http://dx.doi.org/10.5339/connect.2013.14>.
- [2] Ichio Kikuchi and Akihito Kikuchi. Ab-initio quantum chemistry through computer algebra. *Asian Journal of Research and Reviews in Physics*, 6(4):18–31, 2022.
- [3] Ichio Kikuchi and Akihito Kikuchi. Molecular Algebraic Geometry: Electronic Structure of H<sub>3</sub><sup>+</sup> as Algebraic Variety. *OSF Preprints*, 2023. <https://osf.io/preprints/osf/2crxp>.
- [4] Ichio Kikuchi and Akihito Kikuchi. Symbolic, numeric and quantum computation of Hartree-Fock equation. *arXiv preprint arXiv:2401.00019*, 2024.
- [5] Attila Szabo and Neil S Ostlund. *Modern quantum chemistry: introduction to advanced electronic structure theory*. Courier Corporation, 2012.
- [6] S Francis Boys. Electronic wave functions-i. a general method of calculation for the stationary states of any molecular system. *Proceedings of the Royal Society of London. Series A. Mathematical and Physical Sciences*, 200(1063):542–554, 1950.
- [7] David Eisenbud. *Commutative Algebra: with a view toward algebraic geometry*, volume 150. Springer Science & Business Media, 2013.
- [8] David Cox, John Little, and Donal OShea. *Ideals, varieties, and algorithms: an introduction to computational algebraic geometry and commutative algebra*. Springer Science & Business Media, 2013.

- [9] Viviana Ene and Jürgen Herzog. *Gröbner Bases in Commutative Algebra*, volume 130. American Mathematical Soc., 2011.
- [10] Wolfram Decker and Christoph Lossen. Computing in algebraic geometry, volume 16 of algorithms and computation in mathematics, 2006.
- [11] Bruno Buchberger. *An algorithm for finding a basis for the residue class ring of a zero-dimensional polynomial ideal*. PhD thesis, Ph. D. thesis, University of Innsbruck, Austria, 1965.
- [12] Frank Sottile. From enumerative geometry to solving systems of polynomial equations. In *Computations in algebraic geometry with Macaulay 2*, pages 101–129. Springer, 2002.
- [13] Daan Camps and Roel Van Beeumen. Fable: Fast approximate quantum circuits for block-encodings. In *2022 IEEE International Conference on Quantum Computing and Engineering (QCE)*, pages 104–113. IEEE, 2022.
- [14] David Stevenson and Joseph Hirschfelder. The Structure of H<sub>3</sub>, H<sub>3</sub><sup>+</sup>, and of H<sub>3</sub><sup>?</sup>. IV. *The Journal of Chemical Physics*, 5(12):933–940, 1937.
- [15] Joseph O Hirschfelder. The energy of the triatomic hydrogen molecule and ion, V. *The Journal of Chemical Physics*, 6(12):795–806, 1938.
- [16] Harry F King and Keiji Morokuma. Theory of the Rydberg spectrum of triatomic hydrogen. *The Journal of Chemical Physics*, 71(8):3213–3220, 1979.
- [17] Eric Herbst. The astrochemistry of H<sub>3</sub><sup>+</sup>. *Philosophical Transactions of the Royal Society of London. Series A: Mathematical, Physical and Engineering Sciences*, 358(1774):2523–2534, 2000.
- [18] Motomichi Tashiro and Shigeki Kato. Quantum dynamics study on predissociation of H<sub>3</sub> Rydberg states: Importance of indirect mechanism. *The Journal of Chemical Physics*, 117(5):2053–2062, 2002.
- [19] Viatcheslav Kokoouline and Chris H Greene. Theory of Dissociative Recombination of D<sub>3h</sub> Triatomic Ions Applied to H<sub>3</sub><sup>+</sup>. *Physical Review Letters*, 90(13):133201, 2003.
- [20] Takeshi Oka, Thomas R Geballe, Miwa Goto, Tomonori Usuda, and Benjamin J McCall. Hot and diffuse clouds near the galactic center probed by metastable H<sub>3</sub><sup>+</sup>. *The Astrophysical Journal*, 632(2):882, 2005.
- [21] Cina Foroutan-Nejad and Parviz Rashidi-Ranjbar. Chemical bonding in the lightest tri-atomic clusters; H<sub>3</sub><sup>+</sup>, Li<sub>3</sub><sup>+</sup> and B<sub>3</sub><sup>-</sup>. *Journal of Molecular Structure: THEOCHEM*, 901(1-3):243–248, 2009.

- [22] Michele Pavanello, Wei-Cheng Tung, and Ludwik Adamowicz. How to calculate  $h_3$  better. *The Journal of chemical physics*, 131(18):184106, 2009.
- [23] Vikram R Jadhav. Theoretical Approach to Understanding an Electron Density, Charge Density and Most Stable Configuration of  $h_3$  system. *International Journal of Research and Review*, 7(3), 2020.
- [24] Gokul Kannan, Jeremy R Chien, Anthony J Benjamin, Niranjana Bhatia, and Richard J Saykally. Rydberg States of  $H_3$  and  $HeH$  as Potential Coolants for Primordial Star Formation. *The Journal of Physical Chemistry A*, 125(20):4267–4275, 2021.
- [25] Aaron Meurer, Christopher P. Smith, Mateusz Paprocki, Ondřej Čertík, Sergey B. Kirpichev, Matthew Rocklin, AMiT Kumar, Sergiu Ivanov, Jason K. Moore, Sartaj Singh, Thilina Rathnayake, Sean Vig, Brian E. Granger, Richard P. Muller, Francesco Bonazzi, Harsh Gupta, Shivam Vats, Fredrik Johansson, Fabian Pedregosa, Matthew J. Curry, Andy R. Terrel, Štěpán Roučka, Ashutosh Saboo, Isuru Fernando, Sumith Kulal, Robert Cimrman, and Anthony Scopatz. Sympy: symbolic computing in python. *PeerJ Computer Science*, 3:e103, January 2017.
- [26] The Gap Group. GAP - Groups, Algorithms, Programming - a System for Computational Discrete Algebra. Available at <http://www.gap-system.org/>, 2017.
- [27] Hefeng Wang, Lian-Ao Wu, Yu-xi Liu, and Franco Nori. Measurement-based quantum phase estimation algorithm for finding eigenvalues of non-unitary matrices. *Physical Review A*, 82(6):062303, 2010.
- [28] Anmer Daskin, Ananth Grama, and Sabre Kais. A universal quantum circuit scheme for finding complex eigenvalues. *Quantum information processing*, 13:333–353, 2014.
- [29] Changpeng Shao. Computing eigenvalues of diagonalizable matrices on a quantum computer. *ACM Transactions on Quantum Computing*, 3(4):1–20, 2022.
- [30] Miroslav Dobšíček, Göran Johansson, Vitaly Shumeiko, and Göran Wendin. Arbitrary accuracy iterative quantum phase estimation algorithm using a single ancillary qubit: A two-qubit benchmark. *Phys. Rev. A*, 76:030306, Sep 2007.
- [31] Ryan Babbush, Craig Gidney, Dominic W Berry, Nathan Wiebe, Jarrod McClean, Alexandru Paler, Austin Fowler, and Hartmut Neven. Encoding electronic spectra in quantum circuits with linear t complexity. *Physical Review X*, 8(4):041015, 2018.
- [32] Guang Hao Low and Isaac L Chuang. Hamiltonian simulation by qubitization. *Quantum*, 3:163, 2019.

- [33] András Gilyén, Yuan Su, Guang Hao Low, and Nathan Wiebe. Quantum singular value transformation and beyond: exponential improvements for quantum matrix arithmetics. In *Proceedings of the 51st Annual ACM SIGACT Symposium on Theory of Computing*, pages 193–204, 2019.
- [34] David Poulin and Pawel Wocjan. Preparing ground states of quantum many-body systems on a quantum computer. *Physical review letters*, 102(13):130503, 2009.
- [35] Andrew M Childs and Nathan Wiebe. Hamiltonian simulation using linear combinations of unitary operations. *arXiv preprint arXiv:1202.5822*, 2012.
- [36] Dominic W Berry, Andrew M Childs, Richard Cleve, Robin Kothari, and Rolando D Somma. Simulating hamiltonian dynamics with a truncated taylor series. *Physical review letters*, 114(9):090502, 2015.
- [37] David Poulin, Alexei Kitaev, Damian S Steiger, Matthew B Hastings, and Matthias Troyer. Fast quantum algorithm for spectral properties. *arXiv preprint arXiv:1711.11025*, 2017.
- [38] Dominic W Berry, Mária Kieferová, Artur Scherer, Yuval R Sanders, Guang Hao Low, Nathan Wiebe, Craig Gidney, and Ryan Babbush. Improved techniques for preparing eigenstates of fermionic hamiltonians. *npj Quantum Information*, 4(1):22, 2018.
- [39] Yimin Ge, Jordi Tura, and J Ignacio Cirac. Faster ground state preparation and high-precision ground energy estimation with fewer qubits. *Journal of Mathematical Physics*, 60(2), 2019.
- [40] Lin Lin and Yu Tong. Optimal polynomial based quantum eigenstate filtering with application to solving quantum linear systems. *Quantum*, 4:361, 2020.
- [41] A Yu Kitaev. Quantum computations: algorithms and error correction. *Russian Mathematical Surveys*, 52(6):1191, 1997.
- [42] Daniel Gottesman. Theory of fault-tolerant quantum computation. *Physical Review A*, 57(1):127, 1998.
- [43] Austin G Fowler, Matteo Mariantoni, John M Martinis, and Andrew N Cleland. Surface codes: Towards practical large-scale quantum computation. *Physical Review A*, 86(3):032324, 2012.
- [44] Dominic Horsman, Austin G Fowler, Simon Devitt, and Rodney Van Meter. Surface code quantum computing by lattice surgery. *New Journal of Physics*, 14(12):123011, 2012.

- [45] Héctor Bombín. An introduction to topological quantum codes. *arXiv preprint arXiv:1311.0277*, 2013.
- [46] Oscar Higgott. Pymatching: A python package for decoding quantum codes with minimum-weight perfect matching. *ACM Transactions on Quantum Computing*, 3(3):1–16, 2022.
- [47] Lucas Berent, Lukas Burgholzer, Peter-Jan HS Derks, Jens Eisert, and Robert Wille. Decoding quantum color codes with maxsat. *arXiv preprint arXiv:2303.14237*, 2023.
- [48] Yue Wu and Lin Zhong. Fusion blossom: Fast mwpm decoders for qec. In *2023 IEEE International Conference on Quantum Computing and Engineering (QCE)*, volume 1, pages 928–938. IEEE, 2023.
- [49] Bocong Chen, San Ling, and Guanghui Zhang. Application of constacyclic codes to quantum mds codes. *IEEE Transactions on Information Theory*, 61(3):1474–1484, 2015.
- [50] Akshay Degwekar, Kenza Guenda, and T Aaron Gulliver. Extending construction x for quantum error-correcting codes. In *Coding Theory and Applications: 4th International Castle Meeting, Palmela Castle, Portugal, September 15-18, 2014*, pages 141–152. Springer, 2015.
- [51] Nikolas P Breuckmann and Jens Niklas Eberhardt. Quantum low-density parity-check codes. *PRX Quantum*, 2(4):040101, 2021.
- [52] Nicolas Delfosse and Naomi H Nickerson. Almost-linear time decoding algorithm for topological codes. *Quantum*, 5:595, 2021.
- [53] Markus Grassl. Algebraic quantum codes: linking quantum mechanics and discrete mathematics. *International Journal of Computer Mathematics: Computer Systems Theory*, 6(4):243–259, 2021.
- [54] Magali Bardet, Jean-Charles Faugère, and Bruno Salvy. On the complexity of the f5 gröbner basis algorithm. *Journal of Symbolic Computation*, 70:49–70, 2015.

## A Appendix: profiles of the matrices used in the computation

In this section, the structure of transformation matrices used in the main body of the article ( $m_x$ , and  $m_r$ , and  $m_e$ ) are shown by a kind of heat-maps, so that one can see to what extent those matrices are sparse. The entries  $A_{ij}$  in the matrix  $A$  are indicated by 0 or 1 if it is

equal to either of those values; otherwise, they are given by the symbol X. The maximum and the minimum of the entries are also given. The raw numerical data of the matrices are available at <https://github.com/kikuchiichio/20240314>.

`mx:=`

```
|000000X0X0XXX0X0XX0XXX|
|000000X0X0XXX0X0XX0XXX|
|000000X0X0XXX0X0XX0XXX|
|000000X0X0XXX0X0XX0XXX|
|000000X0X0XXX0X0XX0XXX|
|000000X0X0XXX0X0XX0XXX|
|1000000000000000000000|
|000000X0X0XXX0X0XX0XXX|
|0100000000000000000000|
|000000X0X0XXX0X0XX0XXX|
|0010000000000000000000|
|0001000000000000000000|
|0000100000000000000000|
|000000X0X0XXX0X0XX0XXX|
|0000010000000000000000|
|0000001000000000000000|
|0000000100000000000000|
|0000000001000000000000|
|0000000000001000000000|
|0000000000000010000000|
|0000000000000000100000|
|0000000000000000001000|
```

`max(mx)= 258.60441684588295 min(mx)= -72.19094270794328`

`me:=`

```
|XXXXXX0X0X000X0X00X000|
|XXXXXX0X0X000X0X00X000|
|XXXXXX0X0X000X0X00X000|
|XXXXXX0X0X000X0X00X000|
|XXXXXX0X0X000X0X00X000|
|XXXXXX0X0X000X0X00X000|
|000000X0X0XXX0X0XX0XXX|
|0100000000000000000000|
|000000X0X0XXX0X0XX0XXX|
```

```
|001000000000000000000000|
|000000X0X0XXX0X0XX0XXX|
|000000X0X0XXX0X0XX0XXX|
|000000X0X0XXX0X0XX0XXX|
|000001000000000000000000|
|000000X0X0XXX0X0XX0XXX|
|000000010000000000000000|
|000000001000000000000000|
|000000000010000000000000|
|000000000000001000000000|
|000000000000000100000000|
|000000000000000010000000|
|000000000000000001000000|
|000000000000000000100000|
|00000000000000000000100|
max(me)= 4115.255552663199 min(me)= -1486.152450941102
```

mr :=

```
|XXXXXX0X0X000X0X00X000|
|XXXXXX0X0X000X0X00X000|
|XXXXXX0X0X000X0X00X000|
|XXXXXX0X0X000X0X00X000|
|100000000000000000000000|
|010000000000000000000000|
|000000X0X0XXX0X0XX0XXX|
|001000000000000000000000|
|000000X0X0XXX0X0XX0XXX|
|000100000000000000000000|
|000000X0X0XXX0X0XX0XXX|
|000000X0X0XXX0X0XX0XXX|
|000000100000000000000000|
|000000010000000000000000|
|000000001000000000000000|
|000000000100000000000000|
|000000000010000000000000|
|000000000001000000000000|
|000000000000100000000000|
|000000000000010000000000|
|000000000000001000000000|
|000000000000000100000000|
|000000000000000010000000|
|000000000000000001000000|
|000000000000000000100|
```

max(mr)= 3484.3400839743654 min(mr)= -608.2044403624424

## B Hartree-Fock Model

We assume the equilateral triangle model of  $\text{H}_3^+$  (with the bond length  $R$ ) and put atomic bases at three centers A, B, and C.

The trial wave function is given by

$$\psi(r) = x \cdot \phi(r, A) + y \cdot \phi(r, B) + z \cdot \phi(r, C).$$

It is associated with the orbital energy  $e$  and the coefficients  $(x, y, z)$

The atomic orbitals are given by the STO-3G basis set:

$$\phi(r) = \sum_{i=1}^3 d_i \exp(-b_i r^2).$$

In that formula, the parameters are given as

$$b_i = a_i \zeta^2,$$

and

$$d_i = c_i \left( \frac{2b_i}{\pi} \right)^{3/4}$$

for  $i = 1, 2, 3$ . The numeral data are given in Tables 5 and 6.

i	c(i)	a(i)
1	0.4446	0.1098
2	0.5353	0.4058
3	0.1543	2.2277

Table 5: The exponents and coefficients of STO-3G of H.

$\zeta$	1.24
---------	------

Table 6: The scale factor of STO-3G of H.

We write the atomic orbital centered at the site  $X$  as follows:

$$\phi(r, X) = \phi(r - X)$$

We sometimes omit the spatial coordinate  $r$  for simplicity.

We use the following molecular integrals for every possible combination of atomic bases (indexed by the centers of the orbitals: P, Q, and so on). The summations over those indices are taken over orbital centers  $A$ ,  $B$ , and  $C$  in the molecule.

Overlap integrals:

$$S_{PQ} = (\phi(P)|\phi(Q))$$

Kinetic integrals:

$$K_{PQ} = \left( \phi(P) \left| -\frac{1}{2}\nabla^2 \right| \phi(Q) \right)$$

One-center integrals (namely, the nuclear potentials):

$$V_{PQ,U} = - \left( \phi(P) \left| \frac{1}{|r-U|} \right| \phi(Q) \right)$$

Two-center integrals:

$$[PQ | XY] = \int dr_1 dr_2 \phi(r_1, P)\phi(r_1, Q) \frac{1}{|r_1 - r_2|} \phi(r_2, X)\phi(r_2, Y)$$

The skeleton part of the Fock matrix:

$$H_{PQ} = K_{PQ} + V_{PQ,A} + V_{PQ,B} + V_{PQ,C}$$

The density matrix:

$$D = 2 \begin{pmatrix} x^2 & xy & xz \\ xy & y^2 & yz \\ xz & xy & z^2 \end{pmatrix}$$

The electron-electron interaction part of the Fock matrix:

$$G_{PQ} = \sum_{K,L} D_{KL} [PQ | KL] - 0.5 D_{KL} [PL | QK]$$

The Fock matrix:

$$F_{PQ} = K_{PQ} + G_{PQ} + V_{PQ,A} + V_{PQ,B} + V_{PQ,C}$$

The total energy (with the normalization condition and the nuclear-nuclear repulsion):

$$E_{tot} = \frac{1}{2} \sum_{i,j} D_{ij} \cdot (H_{ij} + F_{ij}) - 2e \left( \sum_{i,j} \frac{1}{2} D_{ij} S_{ij} - 1 \right) + \frac{3}{R}$$